

## Ionic Electrets: Electrostatic Charging of Surfaces by Transferring Mobile Ions upon Contact

Logan S. McCarty, Adam Winkleman, and George M. Whitesides\*

*Contribution from the Department of Chemistry and Chemical Biology, Harvard University, 12 Oxford Street, Cambridge, Massachusetts 02138*

Received October 11, 2006; E-mail: gwhitesides@gmwgroup.harvard.edu

**Abstract:** This paper describes the fabrication and characterization of ionic electrets—materials that bear a long-lived electrostatic charge because of an imbalance between the number of cationic and anionic charges in the material. Crosslinked polystyrene microspheres that contain covalently bound ions and mobile counterions transfer some of their mobile ions in air, in the absence of bulk liquid, to another material upon contact. According to the ion-transfer model of contact electrification, this selective transfer of mobile ions yields microspheres that have a net electrostatic charge. A tool that operates on the principle of electrostatic induction measures the charge on individual microspheres (50–450  $\mu\text{m}$  in diameter). Microspheres with a variety of covalently bound ionic functional groups (tetraalkylammonium, alkyltriphenylphosphonium, alkylsulfonate, and arylsulfonate) acquire charges consistent with this ion-transfer mechanism. The charge on a microsphere is proportional to its surface area (ca. 1 elementary charge per 2000  $\text{nm}^2$ ) and close to the theoretical limit imposed by the dielectric breakdown of air. The charge density in an atmosphere of  $\text{SF}_6$  is more than twice that in an atmosphere of  $\text{N}_2$ . These observations suggest that the charge density of these ionic electret microspheres is limited by the dielectric breakdown of the surrounding gas. Functionalizing the surfaces of glass or silicon with covalently bound ions and mobile counterions generates ionic electrets from these inorganic substrates. Soft lithography can pattern charge on a planar silicon surface (with oxide) and on the surface of 250- $\mu\text{m}$  glass microspheres.

### Introduction

This paper describes the fabrication and characterization of ionic electrets—materials that bear a long-lived electrostatic charge because of an imbalance between the number of cationic and anionic charges in the material. By introducing ionic groups into a solid matrix, we can predictably and reproducibly create ionic electrets; these ionic groups must have one type of charge covalently bound and the other mobile. This method works well with crosslinked polystyrene, glass, and silicon (i.e., with the silicon dioxide layer on the surface of silicon). We charge these electrets by contact electrification—the transfer of charge from one surface to another upon contact—using a strategy based on the ion-transfer model hypothesized by Diaz and co-workers.<sup>1–3</sup> Using a tool that operates on the principle of electrostatic induction, we measure the charge on these materials, and demonstrate that the ion-transfer model correctly predicts the sign of their charge. The magnitude of the limiting charge on a spherical ionic electret is proportional to its surface area; the dielectric breakdown of air appears to limit the amount of charge. We also pattern charge on the surface of planar and spherical ionic electrets.

Chemists generally assume that bulk matter is electrically neutral; ionic materials, in particular, are assumed to have an equal number of cationic and anionic charges. This principle

of electroneutrality is taught starting at the beginning of introductory chemistry textbooks.<sup>4</sup> We challenge this assumption by preparing various materials with covalently bound ions and mobile counterions that develop a macroscopic electrostatic charge upon contact with another surface. This charge arises as a result of an imbalance between the number of cationic and anionic charges in (or on) the material that occurs, on contact, when a small number of mobile ions transfer from one surface to the other.

Similar materials find wide application in photocopying and laser printing, and the current understanding of the ion-transfer mechanism of contact electrification comes from studies of toners used in photocopiers.<sup>5</sup> Because contact electrification is a simple and inexpensive technique for creating charged objects, an improved understanding of this phenomenon could lead to wider use of electrostatically charged materials and to the ability to predict, engineer, and pattern regions of net electrostatic charge. Electrostatically charged materials are otherwise prepared by techniques such as bombardment with an electron-beam or ion-beam or by exposure to a corona from a high-voltage electrode.<sup>6</sup> Improved knowledge of the factors that determine contact electrification could also aid in the prevention and control of unwanted charging of materials.<sup>7,8</sup>

(1) Diaz, A. F. *J. Adhes.* **1998**, *67*, 111–122.

(2) Diaz, A. F.; Fenzel-Alexander, D. *Langmuir* **1993**, *9*, 1009–1015.

(3) Diaz, A. F.; Guay, J. *IBM J. Res. Dev.* **1993**, *37*, 249–259.

(4) See, for example: Petrucci, R. M.; Harwood, W. S.; Herring, F. G.; Madura, J. D. *General Chemistry: Principles and Modern Applications*; Pearson Prentice Hall: Upper Saddle River, NJ, 2007.

(5) Pai, D. M.; Springett, B. E. *Rev. Mod. Phys.* **1993**, *65*, 163–211.

## Background

**Properties and Uses of Electrets.** The term *electret* originated in the late 19th century to describe a material that is an electrostatic analogue of a permanent magnet. Although poled electrets have macroscopic electric dipole moments, and are analogous in some sense to permanent magnets, space-charge electrets, which bear a net electrostatic charge, have no magnetic analogue. Classical wax electrets, formed by cooling and solidifying molten wax in a strong electric field, have a macroscopic electric dipole moment due to a net orientation of molecular dipoles; similarly, poly(vinylidene difluoride), PVDF, can be poled by subjecting it to a strong electric field above its glass transition temperature ( $T_g$ ) and cooling it to below  $T_g$  in that field.<sup>6</sup> Space-charge electrets are typically formed by adding charge onto the surface or into the bulk of a material with an electron-beam, an ion-beam, corona discharge from a high-voltage electrode, or direct contact with a charged electrode. These techniques can also pattern charge in an electret.<sup>9–11</sup> Electronic or ionic charges in space-charge electrets may remain on the surface or deeper in the bulk of the material.

Electrets are applied broadly in technologies that make a powder or liquid adhere selectively to another object. After charging the powder, the target object, or both, electrostatic forces guide the powder to coat certain regions of the target. One well-known technology that uses charge-guided patterning is xerography, in which a corona charges a photoconductive imaging drum, light depletes the charge in certain regions, and toner powder (usually charged by contact electrification) adheres specifically to the regions of charge on the drum.<sup>5</sup> Electrostatic separation technologies can separate coal from various impurities, and separate powders composed of different types of plastic for recycling.<sup>12,13</sup> Electrostatic powder coating and electrostatic spray painting coat large objects with a uniform layer of plastic powder or paint;<sup>14,15</sup> similar techniques apply powdered flavorings and salt to potato chips<sup>16</sup> and popcorn.<sup>17</sup> (Our recent demonstration of electrostatic self-assembly of chemically modified polystyrene microspheres<sup>18</sup> is similar to electrostatic powder coating, though on a much smaller size scale.) Other applications of electrets include electret microphones, in which the acoustical vibration of a thin electret membrane induces voltage fluctuations between two electrodes,<sup>6</sup> and Van de Graaff generators, which rely on the storage and transport of charge on an electrically insulating belt.<sup>19</sup>

There are many instances in which electrostatic charging must be avoided. Helicopter blades (and helicopters) develop sub-

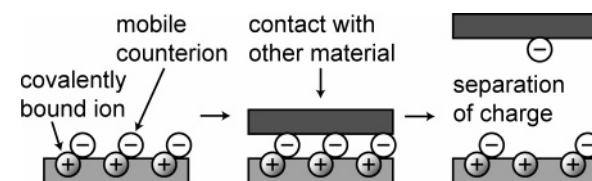


**Figure 1.** Schematic illustration of the ion-transfer mechanism of contact electrification.

stantial electrical charge when moving through air; this charge can be lethal if a person approaches an ungrounded helicopter that is near the ground.<sup>20</sup> The flow of liquids or powders through pipes often leads to electrostatic charging. This charging can be a substantial hazard with pharmaceutical powders<sup>21</sup> or hydrocarbon fuels.<sup>7,22</sup> The charge accumulated on a person's body in a low-humidity environment is sufficient to destroy sensitive electronic equipment.<sup>8,23,24</sup>

**The Ion-Transfer Model of Contact Electrification.** When two solid surfaces are brought into contact and separated (with or without rubbing), charge is often transferred from one surface to the other in a process known as “contact electrification” or “tribocharging”.<sup>25,26</sup> Despite its economic significance (both beneficial and harmful), contact electrification remains poorly understood, especially at the molecular or atomic level. Even the most fundamental question of whether the charge carrier is an electron or an ion is still under debate.<sup>3,25–37</sup> Nearly all materials (metals, semiconductors, and insulators) undergo contact electrification under a wide range of environmental conditions; it is likely that different mechanisms of electrification dominate in different circumstances. There are two kinds of materials for which there is general agreement on the mechanism of contact electrification: (i) contact between two different metals results in the transfer of electrons owing to the difference in work functions of the metals,<sup>38</sup> and (ii) any contact with a material that has covalently bound ions and mobile counterions results in the transfer of some of the mobile ions to the contacted surface.<sup>1</sup> Diaz and co-workers investigated the latter process and developed the ion-transfer model of contact electrification, shown schematically in Figure 1.<sup>2,3</sup>

The ion-transfer model makes two qualitative predictions. First, the sign of charge acquired by the ionic material (the ionomer) should be the same as the sign of the covalently bound ion. Second, the mobile ion should be observed on the other surface after contact. Diaz confirmed both predictions using

- (6) *Electrets*; Sessler, G. M., Gerhard-Multhaupt, R., Eds.; Laplacian Press: Morgan Hill, CA, 1998.
- (7) Gibson, N. J. *Electrostat.* **1997**, 40–41, 21–30.
- (8) Greason, W. D. *IEEE Trans. Ind. Appl.* **1987**, 23, 205–216.
- (9) Jacobs, H. O.; Whitesides, G. M. *Science* **2001**, 291, 1763–1766.
- (10) Mikihiro, K.; Norio, S.; Takehiro, D.; Hiroshi, F.; Takeshi, K.; Mitsuru, E. *Proc. SPIE-Int. Soc. Opt. Eng.* **2001**, 4334, 263–270.
- (11) Rezek, B.; Stuchlik, J.; Kocka, J.; Stemmer, A. *J. Non-Cryst. Solids* **2005**, 351, 3127–3131.
- (12) Kwetkus, B. A. *Particulate Sci. Technol.* **1998**, 16, 55–68.
- (13) Higashiyama, Y.; Asano, K. *Particulate Sci. Technol.* **1998**, 16, 77–90.
- (14) Richart, D. S. In *Kirk-Othmer Encyclopedia of Chemical Technology*, 4th ed.; Kroschwitz, J. I., Howe-Grant, M., Eds.; Wiley: New York, 1992; Vol. 6, pp 635–661.
- (15) Bailey, A. G. *J. Electrostat.* **1998**, 45, 85–120.
- (16) Ratanatriwong, P.; Barringer, S.; Delwiche, J. J. *Food Sci.* **2003**, 68, 1542–1547.
- (17) Miller, M. J.; Barringer, S. A. *J. Food Sci.* **2002**, 67, 198–201.
- (18) McCarty, L. S.; Winkleman, A.; Whitesides, G. M. *Angew. Chem., Int. Ed.* **2006**, 46, 206–209.
- (19) Halliday, D.; Resnick, R.; Walker, J. *Fundamentals of Physics*; J. Wiley & Sons: Hoboken, NJ, 2005.

- (20) Felici, N.; Larigaldie, S. J. *Electrostat.* **1980**, 9, 59–70.
- (21) Bailey, A. G. *Powder Technol.* **1984**, 37, 71–85.
- (22) Morrison, I. D. *Colloids Surf. A* **1993**, 71, 1–37.
- (23) Davies, D. K. J. *Electrostat.* **1985**, 16, 329–342.
- (24) Crockett, R. G. M.; Hughes, J. F.; Pude, J. R. G.; Sno, H. M. *J. Electrostat.* **1985**, 16, 343–352.
- (25) Harper, W. R. *Contact and Frictional Electrification*; Laplacian Press: Morgan Hill, CA, 1998.
- (26) Lowell, J.; Rose-Innes, A. C. *Adv. Phys.* **1980**, 29, 947–1023.
- (27) Medley, J. A. *Nature* **1953**, 171, 1077–1077.
- (28) Davies, D. K. J. *Phys. D: Appl. Phys.* **1969**, 2, 1533–1537.
- (29) Lee, L. H. *Photog. Sci. Eng.* **1978**, 22, 228–231.
- (30) Duke, C. B.; Fabish, T. J. *J. Appl. Phys.* **1978**, 49, 315–321.
- (31) Gibson, H. W. *Polymer* **1984**, 25, 3–27.
- (32) Anderson, J. H. *J. Imaging Sci.* **1989**, 33, 200–203.
- (33) Sakaguchi, M.; Shimada, S.; Kashiwabara, H. *Macromolecules* **1990**, 23, 5038–5040.
- (34) Horn, R. G.; Smith, D. T.; Grabbe, A. *Nature* **1993**, 366, 442–443.
- (35) Clint, J. H.; Dunstan, T. S. *Europhys. Lett.* **2001**, 54, 320–322.
- (36) Hoshino, K.; Ohoka, H.; Kokado, H.; Kitamura, T. *Macromol. Chem. Phys.* **2001**, 202, 367–374.
- (37) Grzybowski, B. A.; Fialkowski, M.; Wiles, J. A. *J. Phys. Chem. B* **2005**, 109, 20511–20515.
- (38) Harper, W. R. *Proc. R. Soc. London, Ser. A* **1951**, 205, 83–103.

materials that were made by melt-mixing a styrene-butyl methacrylate random copolymer with various ionomers, such as poly(*N*-methylvinylpyridinium toluenesulfonate). These materials served as models for xerographic toners;<sup>39</sup> they were milled and sorted by size to yield ca. 10- $\mu$ m particles. Diaz and co-workers measured the contact electrification of these powders using a “blow-off” Faraday cage commonly used in the photocopying industry,<sup>40</sup> and found that the sign of charge agreed with the predictions of the ion-transfer model. He used X-ray photoelectron spectroscopy to demonstrate transfer of the mobile ion but not the covalently bound ion following contact.<sup>41</sup> Other researchers also observed that ion-transfer accompanied the contact electrification of polymers doped with various organic salts.<sup>42,43</sup>

The ion-transfer model, in its most basic form, does not make any predictions about the magnitude of charge expected from contact electrification. There are physical limitations on the amount of charge that can be stored on an electret: when the electric field at the surface of the electret exceeds certain limits, dielectric breakdown of the surrounding gas, or field emission in a vacuum, will partially discharge the electret.<sup>6,25,44</sup> Previous studies of the magnitude of charge attained by contact electrification had several limitations. The “blow-off” Faraday cage measures the charge per unit *mass* of bulk powder, while the charge per unit *area* determines the electric field at the surface. Melt-mixed polymer powders, though relevant as a model for toner, likely exhibit phase segregation, an unknown surface composition, and uncontrolled surface morphology.

## Experimental Design

We had five experimental objectives. (i) We wanted to test the usefulness of the ion-transfer model of contact electrification in the design of materials that develop a certain sign of charge upon contact. Chloromethylated crosslinked polystyrene microspheres (Merrifield resin) offered a versatile matrix on which we could generate various ionic functional groups. Upon contact with another surface, microspheres with bound cations became positively charged, while microspheres with bound anions became negatively charged. (ii) We wanted to measure the charge per unit area of these ionic electret materials. Using a tool specifically developed for this purpose that can measure the electrostatic charge on single microspheres, we measured charge as a function of surface area for microspheres with diameters of 50–450  $\mu$ m. (iii) We wanted to determine the maximum charge that an electret can acquire through contact electrification and identify the factors that influence this maximum charge. By comparing the maximum charge of electret microspheres containing various ionic groups under various conditions (different humidity, various gases), we found that the dielectric breakdown of air or the surrounding gas limits the maximum stable charge on a spherical electret. (iv) We wanted to make ionic electrets from materials other than polymers. The surfaces of glass and silicon, functionalized with

silanes containing covalently bound ions and mobile counterions, acquired charge upon contact, in accord with the ion-transfer model. (v) We wanted to demonstrate that ionic electrets could be prepared with a pattern of charge. Using the techniques of soft lithography,<sup>45</sup> we patterned charge on planar silicon surfaces and on glass microspheres and imaged the patterns of charge using Kelvin probe force microscopy (KFM)<sup>46–48</sup> and electrostatic self-assembly.<sup>18</sup>

## Results and Discussion

**Fabrication of Ionic Electrets from Polystyrene Microspheres.** Scheme 1 shows our approach to the functionalization of monodisperse crosslinked polystyrene microspheres of various sizes. After chloromethylating the polystyrene spheres,<sup>49</sup> we introduced various ionic functional groups, such as tetraalkylammonium (**1**), sulfonate (**2**), and alkyltriphenylphosphonium (**3**). We also used a sulfonated azobenzene moiety (**4**).<sup>18</sup> The degree of functional group substitution was sufficiently low ( $\sim 5$  to 10% of the styrene residues) that these polystyrene resins remained hydrophobic: they did not swell in water (unlike typical ion-exchange resins). Because there is a suggestion in the literature that water might play a role in the ion-transfer mechanism of contact electrification,<sup>50</sup> we prepared derivatives with both hydrophilic counterions (sodium or chloride) and hydrophobic counterions (tetraphenylphosphonium or tetraphenylborate) using ion exchange.

**A Tool for Measuring the Charge on Ionic Electret Microspheres.** We designed and built a tool that can measure the electrostatic charge on single microspheres. Figure 2a shows the basic design of the tool; Figure S5 in the Supporting Information has a photograph. This tool consists of four concentric cylinders: a central polyethylene tube surrounded by two aluminum cylinders (electrically insulated from each other), all enclosed inside a grounded steel cylinder that shields the device from stray electric fields. A shielded triaxial cable connects the two aluminum cylinders to an electrometer. One end of the polyethylene tube is connected to house vacuum, while the other end is open to the atmosphere. When the open end of this tube is brought near a charged bead, the flow of air draws the bead through the polyethylene tube.

The electrometer, in charge-measurement mode, acts as an integrating ammeter: it maintains the two aluminum cylinders at the same electrical potential and measures the total flow of charge (the time integral of the current) between them. The electrometer averages this charge over a period of 1/60 of a second and records the average charge. Because there are no free charges in the space between the cylinders, the potential in that region is described by Laplace's equation. The constant electrostatic potential on the boundary yields a unique solution: a constant electrostatic potential throughout the region between the cylinders. This constant potential means that there is no electric field in the space between the cylinders, so the total flux of the electric field through a cylindrical Gaussian

(39) Macholdt, H. T.; Sieber, A. J. *Imaging Technol.* **1988**, *14*, 89–93.

(40) Schein, L. B. *Electrophotography and Development Physics*; Laplacian Press: Morgan Hill, CA, 1996.

(41) Diaz, A. F.; Wollmann, D.; Dreblow, D. *Chem. Mater.* **1991**, *3*, 997–999.

(42) Mizes, H. A.; Conwell, E. M.; Salamida, D. P. *Appl. Phys. Lett.* **1990**, *56*, 1597–1599.

(43) Law, K. Y.; Tarnawskyj, I. W.; Salamida, D.; Debies, T. *Chem. Mater.* **1995**, *7*, 2090–2095.

(44) Meek, J. M.; Craggs, J. D. *Electrical Breakdown of Gases*; Clarendon Press: Oxford, 1953.

(45) Xia, Y. N.; Whitesides, G. M. *Angew. Chem., Int. Ed.* **1998**, *37*, 551–575.

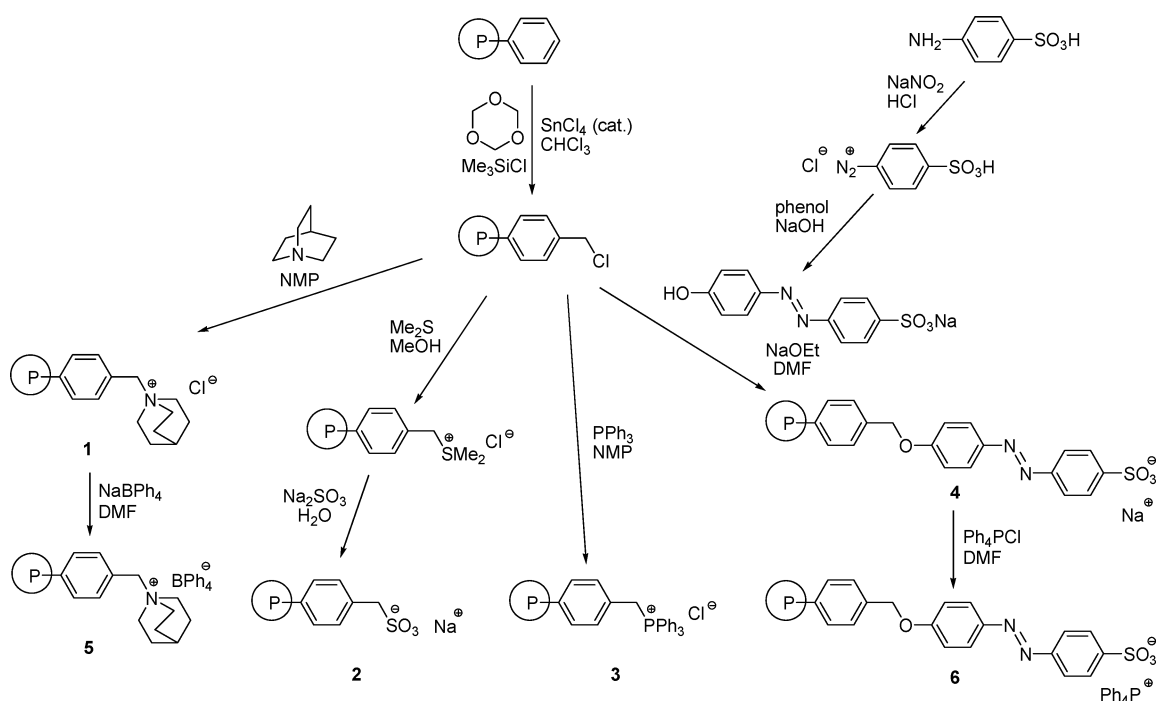
(46) Martin, Y.; Abraham, D. W.; Wickramasinghe, H. K. *Appl. Phys. Lett.* **1988**, *52*, 1103–1105.

(47) Nonnenmacher, M.; Oboyle, M. P.; Wickramasinghe, H. K. *Appl. Phys. Lett.* **1991**, *58*, 2921–2923.

(48) Jacobs, H. O.; Knapp, H. F.; Stemmer, A. *Rev. Sci. Instrum.* **1999**, *70*, 1756–1760.

(49) Itsuno, S.; Uchikoshi, K.; Ito, K. *J. Am. Chem. Soc.* **1990**, *112*, 8187–8188.

(50) Pence, S.; Novotny, V. J.; Diaz, A. F. *Langmuir* **1994**, *10*, 592–596.

**Scheme 1.** Synthetic Scheme for the Functionalization of Crosslinked Polystyrene to Yield Ionic Electrets with Various Ionic Functional Groups<sup>a</sup><sup>a</sup> The Experimental Section provides experimental details.

surface constructed between the inner and outer cylinders must be zero. By Gauss's Law, the total charge on the inner cylinder and any of its contents (e.g., a charged bead) will always be zero. When a positively charged bead enters the central aluminum cylinder, electrons flow from the outer cylinder to the inner cylinder (Figure 2b) in order that the *total* charge on the inner cylinder plus the bead remains equal to zero. The amount of charge that flows through the electrometer is equal to the charge on the bead. When the bead exits the inner cylinder, these induced charges flow back through the electrometer. The device makes two measurements of charge for each bead: first, when the bead enters the inner cylinder, and second, when the bead exits the cylinder.

Ideally, a graph of charge as a function of time for a single bead should yield a symmetric square-shaped peak. Figure 3a shows an example of an actual peak. The internal averaging of the electrometer results in some interpolated data points, such as the one marked with an asterisk in the figure. The width of the square peak indicates the length of time ( $\sim 60$  microseconds) required for the bead to traverse the central aluminum cylinder (a distance of 1 meter). The charge on the bead when it enters the device (the leading-edge charge) is equal to the difference between the top of the peak and the initial baseline, while the charge on the bead when it exits the device (the lagging-edge charge) is equal to the difference between the top of the peak and the final baseline. Note that the baseline shifts: the leading-edge charge is not equal to the lagging-edge charge. Apparently, the bead emerges with a different charge than it had when it entered. We believe that the bead collides with the walls of the polyethylene tube as it travels through the device, and these collisions result in contact electrification reflecting transfer of charge between the bead and the tube. The flow of air through the device is turbulent (average velocity  $\sim 70$  m/s, for a Reynolds number of  $\sim 6000$ ), and the tube is not perfectly straight, so

such collisions are likely. As we shall discuss later, however, this baseline shift is not statistically significant.

Measuring the flow of charge between two concentric cylinders, rather than measuring the charge induced on one electrode relative to ground, helps to minimize the inevitable noise and charge fluctuations of the ground. The digital electrometer has a precision of 10 fC ( $\sim 60\,000$  elementary charges); the baseline rms noise (peak-to-peak) of our device was less than 20 fC. The smallest beads that we measured ( $50\text{-}\mu\text{m}$  diameter) had charges that were ca. 40 times the rms noise.

We scrutinized any peaks that lay more than three standard deviations from the mean for a given sample of beads and would exclude a peak from our analysis of the data in two situations. Sometimes, more than one bead would pass through the device at the same time. We usually noticed these events during the collection of data, and the resulting peaks had multiple plateaus, as shown in Figure 3b. These peaks were higher than the other peaks, and had a total charge that was a whole-number multiple of the charge on a single bead. At other times, a bead would pass through the device so rapidly that the electrometer, with its internal averaging, would not capture the full charge of the bead. Since a very narrow square peak, upon averaging, yields a much lower triangular peak, these events would lead to peaks with only a single data point at the apex, and an unusually low charge. Using both of these criteria, we rejected about 5% of the peaks collected in any given experiment. We retained any statistical outliers that did not have an obviously erroneous peak shape.

Figure 4a shows an example of the raw output from the electrometer for measurements of charge of 41 positively charged,  $200\text{-}\mu\text{m}$ -diameter beads with alkytriphenylphosphonium functionality (3). We eliminated one peak from the data because it had an unusually low charge and only a single data point at its apex. The peaks have various widths, indicating that



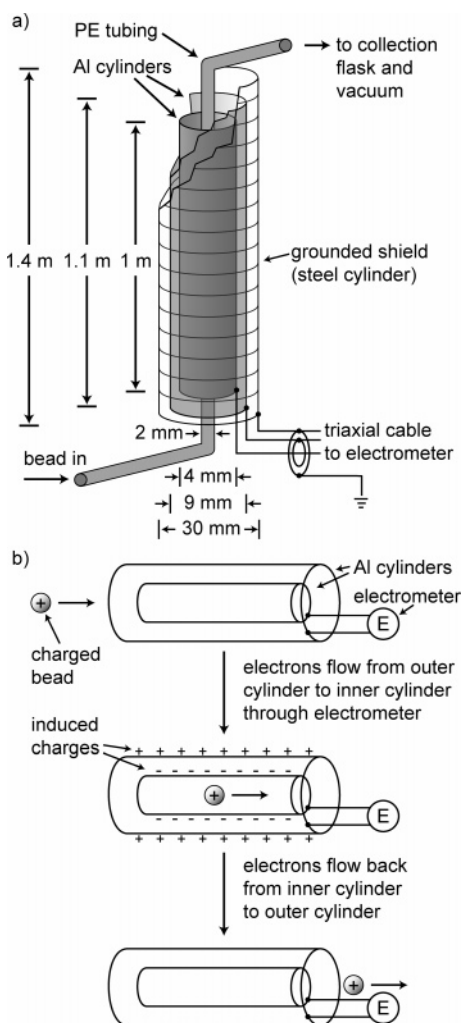


**Figure 2.** (a) Schematic illustration of the apparatus used for measuring the charge on individual microspheres; (b) schematic of the process by which the apparatus measures the charge on a microsphere.

beads traverse the device at different average speeds. The turbulent flow of air and random collisions between the bead and the tube are consistent with this observation. The width of each peak is not correlated with the charge measured for that bead. The heights of the peaks appear to be similar. Both baseline shift (bead-to-bead) and overall baseline drift are evident.

A simple peak-finding algorithm calculated the leading-edge charge and the lagging-edge charge for each peak. Figure 4 parts b, c, and d show histograms of the leading-edge charge, the lagging-edge charge, and the average charge, respectively, for the 41 beads measured in Figure 4a. The differences between the mean charges determined by these three methods are not statistically significant, as confirmed by paired *t*-tests. For consistency in comparing different experiments, we used only the leading-edge charge, which better represents the charge on the bead when it enters the device and is more informative, we believe, than the other measures of charge. We present histograms to highlight any statistical outliers: in particular, we wish to draw attention to any beads that had a different sign of charge from the other beads in a sample. (Later in this paper, we will provide evidence that the broad distributions of charge seen in these histograms indicate an actual distribution of

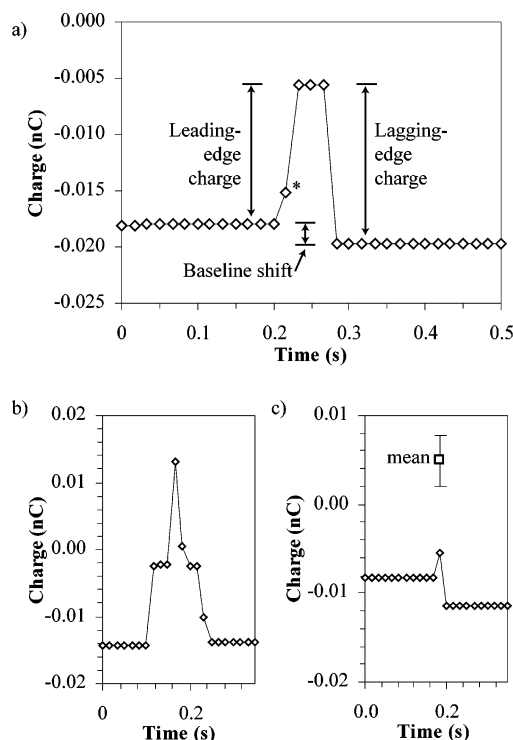


**Figure 3.** (a) An example of a peak resulting from the passage of a single positively charged bead through the apparatus. The leading-edge charge, lagging-edge charge, and baseline shift are indicated. The datum indicated with an asterisk (\*) is an artifact of the internal averaging used by the electrometer. (b) An example of a peak resulting from the passage of two positively charged beads together through the apparatus. Such a peak would be excluded from the data analysis. (c) An example of a peak with only a single datum at its apex that resulted from the very rapid passage of a single positively charged bead through the apparatus. The mean and standard deviation of other beads in the same sample is indicated; the observed peak falls more than three standard deviations below the mean. Such a peak would also be excluded from the analysis.

charges on the beads, and are not mere artifacts of the uncertainty of our measuring device.)

Figure 5a shows measurements of the reproducibility of our charge-measuring device using 200- $\mu$ m-diameter beads having immobilized tetraalkylammonium cations and mobile anions (1). Measurements of three different samples of these beads on a single day yielded mean charges that were statistically indistinguishable. Measurements made on three other days, over a span of 7 months, under various ambient conditions of temperature and humidity, had statistically significant differences. When we sought quantitative comparisons between different batches of beads, we measured the various beads on a single day to ensure that these comparisons would be statistically meaningful. Measurements made on different days are reproducible to within about one standard deviation (ca. 25% of the mean charge). We show later that differences in the ambient humidity can explain the variations in the amounts of charge observed on different days.

Following the procedure used in our previous communication,<sup>18</sup> we charged the electret beads by placing them in an aluminum dish and manually agitating the dish at a frequency of  $\sim 3$  Hz for  $\sim 1$  min before making the measurements of charge. (We later found that extensive agitation was not necessary. As we discuss in the next paragraph, the brief contact between the beads and the polyethylene tube inside the charge-measuring device imparted substantial charges to these beads.)

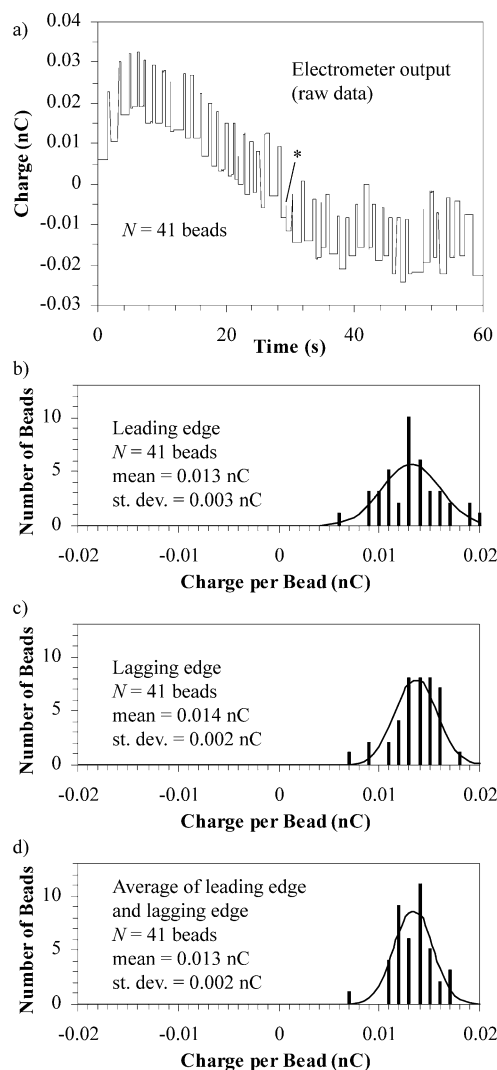


**Figure 4.** (a) The electrometer output from the measurement of 41 positively charged 200- $\mu\text{m}$ -diameter beads with alkyltriphenylphosphonium functionality (**3**); contact with aluminum charged the beads. The peak indicated with an asterisk (\*) was excluded from the data analysis for reasons explained in the text. (b–d) Histograms of the measurements of charge extracted from the electrometer output shown above; the superimposed curve is the normal distribution calculated from the mean and standard deviation: (b) the leading-edge charge, (c) the lagging edge charge, and (d) the average of the leading-edge and lagging-edge charge.

Figure 5b compares the results of using various other materials for the contact electrification of these beads. The beads were agitated in a glass vial, or rolled between two sheets of polymer film—polyethylene (PE), poly(hexamethylene adipamide) (Nylon-6,6), or poly(tetrafluoroethylene) (PTFE)—before making the measurements of charge. Although the differences between some of these measurements are statistically significant, the general magnitude of charge is the same; more importantly, the sign of charge is always the same. In particular, the similar results for Nylon and PTFE, two materials that are at opposite ends of the “triboelectric series”,<sup>25,51,52</sup> suggest that the ion-transfer mechanism of contact electrification for ionic electrets overrides any intrinsic triboelectric properties of the contacted material. The introduction of covalently bound ions and mobile counterions yields predictable electrification upon contact with a wide variety of materials.

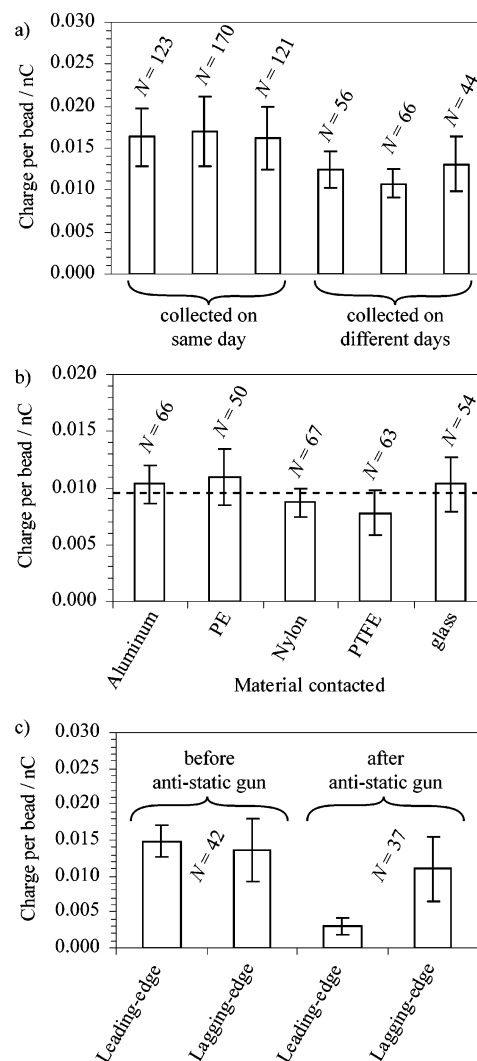


**Figure 5.** (a) Comparisons of the measurements of charge (mean, standard deviation, and number of beads  $N$ ) for different samples of 200- $\mu\text{m}$ -diameter tetraalkylammonium beads (**1**) obtained on a single day or on different days. Contact with aluminum charged the beads. (b) Comparisons of the measurements of charge (from a single day) for different samples of 200- $\mu\text{m}$ -diameter tetraalkylammonium beads (**1**) charged by contact electrification against various materials. The dashed line indicates the mean of the means. (c) Measurements (on a single day) showing the effect of an antistatic gun (ZeroStat) on the charge of 200- $\mu\text{m}$ -diameter tetraalkylammonium beads (**1**) charged by contact electrification against polyethylene. (Figures S1, S2, and S3 in the Supporting Information provide histograms of all the data shown in this figure.)

We sprayed beads with neutralizing ions from an antistatic gun (ZeroStat) and measured their charge. Figure 5c shows the measurements of charge before and after this antistatic treatment. The neutralizing ions reduced the charge on the beads (measured at the leading edge) to 20% of their full charge. The charge measured at the lagging edge, however, was nearly the same for samples that had been treated with the antistatic gun and those that had not been treated. This observation confirms that contact with the polyethylene tube charges the bead as it passes through the charge-measuring device. Evidently, there is sufficient contact between the bead and the 1-meter-long tube to charge the bead to  $\sim 80\%$  of its full charge; this contact occurs over a duration of 15–150 milliseconds (the range of transit times observed for this sample of beads). This observation is consistent with our hypothesis that the turbulent flow of air

(51) Diaz, A. F.; Felix-Navarro, R. M. *J. Electrostat.* **2004**, *62*, 277–290.

(52) Henniker, J. *Nature* **1962**, *196*, 474.

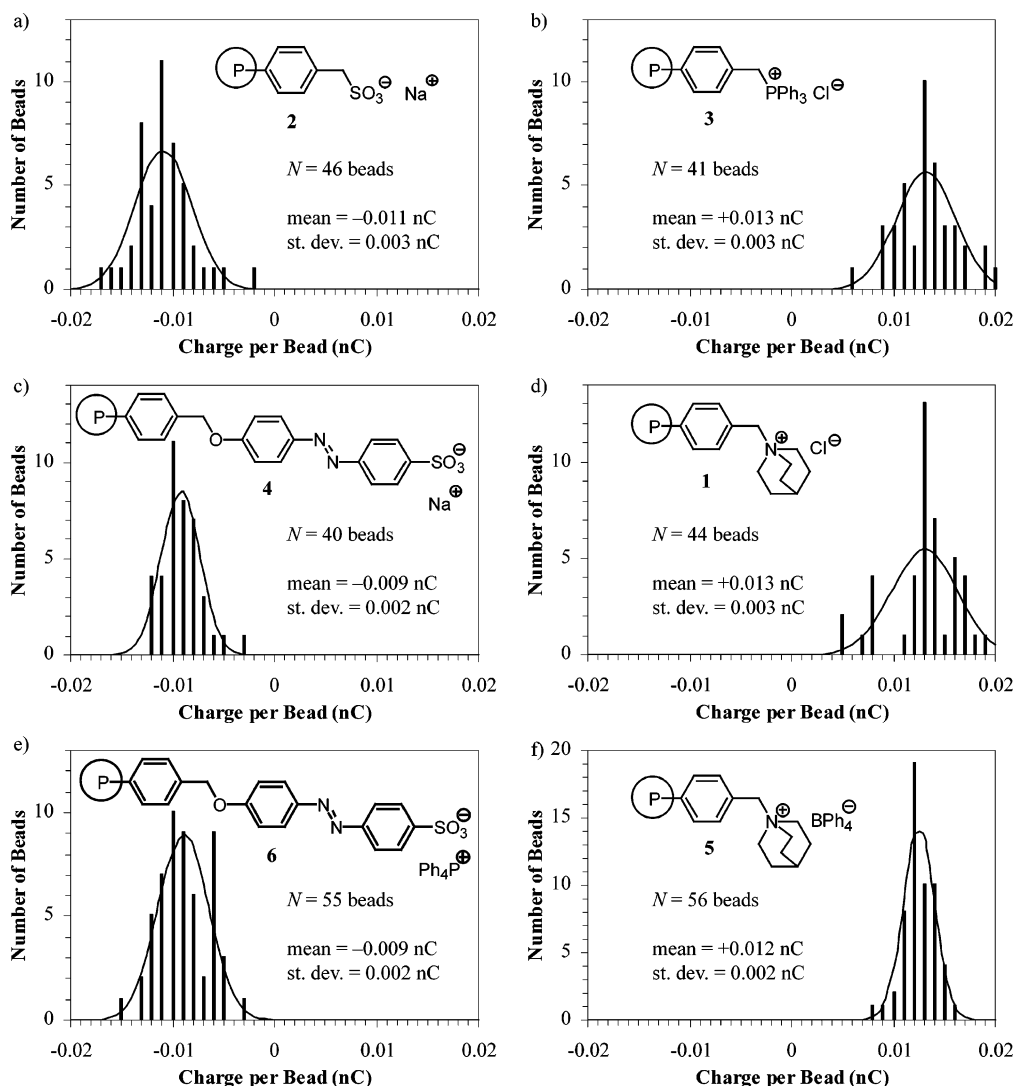


**Figure 6.** Histograms (charge per bead) for functionalized polystyrene beads (200- $\mu\text{m}$  diameter) charged by contact with aluminum. The superimposed curves show the normal distributions calculated from the mean and standard deviation of each set of data.

inside the tube leads to repeated collisions between the bead and the walls of the tube.

**The Charge on Various Ionic Electrets Is Consistent with the Ion-Transfer Model.** Figure 6 shows histograms of charge measurements for 200- $\mu\text{m}$ -diameter microspheres with various ionic functional groups. Every bead had the same sign of charge as the covalently bound ion, as predicted by the ion-transfer model of contact electrification. No beads were uncharged. Changes in the functional group or the counterion did not lead to significant differences in the amount of charge. These results indicate that the ion-transfer model offers a predictable and rational approach to materials that will become electrostatically charged upon contact. It is difficult to see how an electron-transfer mechanism can explain these results. For instance, we observed the same sign and magnitude of contact electrification when we replaced the chloride anion (**1**) with the tetraphenylborate anion (**5**), even though the latter is a far better electron donor.

The magnitude of charge ( $\sim 0.01$  nC per bead) was similar for both positively charged and negatively charged microspheres. Assuming that the charge is distributed uniformly on the surface of each bead, the magnitude of charge corresponds to ca. one elementary charge per 2000  $\text{nm}^2$ . On the basis of the degree of

functionalization of these microspheres, we estimate that there is roughly one functional group per 10  $\text{nm}^2$  of surface, so contact electrification appears to separate only a small fraction ( $\sim 0.5\%$ ) of the mobile counterions on the surface from their covalently bound partners. We obtained similar measurements of charge for beads that had been stored in air for several months or for beads that had already been passed once through the charge-measuring device.

**The Charge on a Spherical Ionic Electret Is Proportional to Its Surface Area.** We measured the charge on tetraalkylammonium-functionalized microspheres (**1**) with diameters of 50, 100, 200, and 450  $\mu\text{m}$ . The inset in Figure 7a shows the linear correlation between the charge on a bead and its surface area; because two of the data cluster near the origin, we show on the larger graph the correlation between the square root of the charge and the diameter of the bead. (Compared with the other beads, the 450- $\mu\text{m}$  beads had greater polydispersity in size, which could contribute to the larger standard deviation in their charge.) All beads had roughly the same surface charge density, ca. 1 elementary charge per 2000  $\text{nm}^2$ . Although the ion-transfer model of contact electrification does not specifically predict that charge should be proportional to surface area, this observation is not surprising for a process that takes place at a surface.

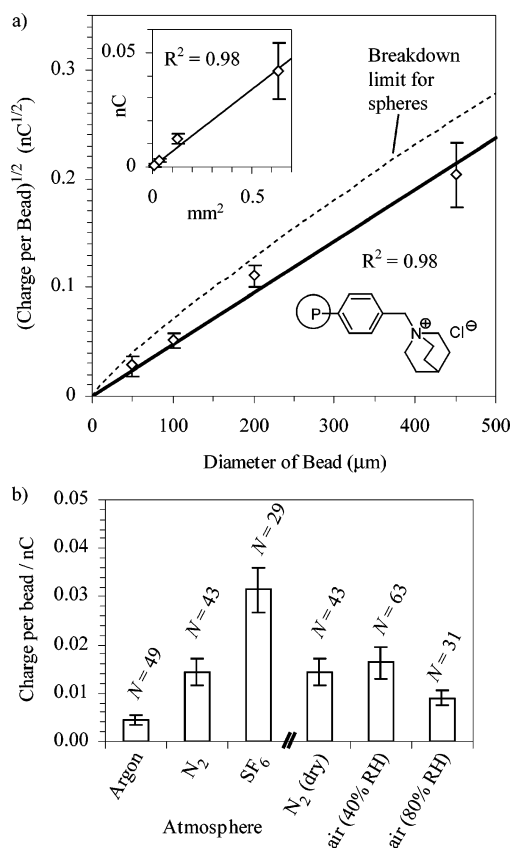


**Figure 7.** (a) Linear correlation between the square root of the bead charge and the diameter of the bead. (All beads had tetraalkylammonium functionality **1** and were charged by contact with aluminum; measurements were made on a single day.) The dashed line indicates the surface charge (calculated using eq 1) that would lead to dielectric breakdown of air around a small charged sphere. The inset shows the linear correlation between the bead charge and the surface area of the bead. (b) Measurements of charge for 200- $\mu\text{m}$ -diameter tetraalkylammonium beads (**1**) charged by contact with aluminum in a polyethylene bag purged with argon,  $\text{N}_2$ , or  $\text{SF}_6$  gases, or at various levels of humidity (dry nitrogen, 40% RH, or 80% RH).

**The Maximum Charge on a Spherical Ionic Electret Is Limited by the Dielectric Breakdown of the Surrounding Medium.** The maximum stable charge on an electret is typically determined by the process of dielectric breakdown—the flow of current through an otherwise insulating material owing to cascading ionization in a high electric field.<sup>6,25,44</sup> Charge on the surface of an insulating sphere can be discharged by two methods: (i) through a gas (by dielectric breakdown of the gas), or (ii) upon contact with another surface because of some conductivity (presumably, in this case, ionic) on the surface of the sphere. In the case of gaseous breakdown, charge on the sphere will flow through the ionized gas to some other material that need not be in contact with the sphere. In the case of surface conductivity, charge can flow along the surface of the sphere and dissipate onto a material in contact with the sphere. As we shall discuss, the adsorption of water at high ambient humidity increases the surface conductivity of most materials.<sup>53</sup>

The threshold for dielectric breakdown of air in a uniform electric field is approximately 30 kV/cm.<sup>44</sup> Applying this criterion to our electrets, and assuming that the charge is uniformly distributed on the spherical surface, we would predict a limiting charge density of 1 charge per 6000  $\text{nm}^2$ ; our electrets

have charge densities about three times that limit. The electric field around a spherical distribution of charge depends only on the total charge inside the sphere (by Gauss's law), and does not depend on whether the charge is on the surface or in the interior of the sphere.<sup>19</sup> According to Harper,<sup>25</sup> electric fields stronger than 30 kV/cm will not cause dielectric breakdown if the high field is confined to a small region of space. Because the magnitude of the electric field at a distance  $r$  from the center of a charged sphere diminishes in proportion to  $1/r^2$ , a small charged sphere will have a strong electric field only near its surface. In addition, since the electric field around a spherical distribution of charge depends only on the total charge inside the sphere, the dielectric constant or other properties of the sphere itself do not affect the electric field at the surface or the propensity for dielectric breakdown. Harper proposed that the minimum electric field that will cause dielectric breakdown around a small charged sphere in dry air is empirically described by the formula in eq 1 ( $r$  = radius in cm):

$$E = 37(r/\text{cm})^{-0.3} \text{ kV/cm} \quad (1)$$

The dashed line in Figure 7a shows the limiting charge calculated using this formula. (The limiting charge is not exactly proportional to the surface area: small beads can sustain a higher electric field than large beads.) The average charge on our ionic electrets is close to this breakdown limit, which suggests that the dielectric breakdown of air determines the ultimate limit of the stable charge on these materials: any charge separation beyond this limit would result in a discharge. This hypothesis may explain why we observe only a small fraction of the charge that could be attained if every mobile ion were transferred during contact electrification.

Different gases have different thresholds for dielectric breakdown.<sup>54</sup> Dry air, humid air, oxygen, nitrogen, and carbon dioxide all have similar dielectric strengths. The noble gases have dielectric strengths that are much lower than that of air (argon, for instance, has a dielectric strength about one-fourth that of air). Halogenated gases such as  $\text{CCl}_4$ , chlorofluorocarbons, and  $\text{SF}_6$  have the highest dielectric strengths ( $\text{SF}_6$  has a dielectric strength about 2.5 times that of air). We compared the charges attained by ionic electrets in atmospheres of argon, nitrogen, and  $\text{SF}_6$  (Figure 7b). The beads charged in argon had charges about one-third that of beads charged in nitrogen, while the beads charged in  $\text{SF}_6$  had charges more than twice that of beads charged in nitrogen. Although we cannot compare these ratios quantitatively with the relative dielectric strengths determined in uniform electric fields (the relative dielectric strengths of various gases depend on the geometry of the electric field), the general trend is consistent with our hypothesis: dielectric breakdown of the surrounding gas determines the maximum charge on these ionic electret microspheres. Since the strength of the electric field causes dielectric breakdown, and the electric field outside a charged sphere depends only on the charge inside the sphere, the dielectric breakdown of air (or the surrounding medium) would presumably impose a similar limit on all spherical electrets. (Dielectric breakdown imposes an ultimate limit on the stable charge of *all* electrets,<sup>6</sup> but the electric field strength for nonspherical geometries depends on the specific charge distribution and dielectric properties of the materials.)

(53) Seaver, A. E. *J. Electrostat.* **2005**, *63*, 203–222.

(54) Blair, D. T. A. In *Electrical Breakdown of Gases*; Meek, J. M., Craggs, J. D., Eds.; John Wiley and Sons: Chichester, U.K., 1978; pp 533–653.



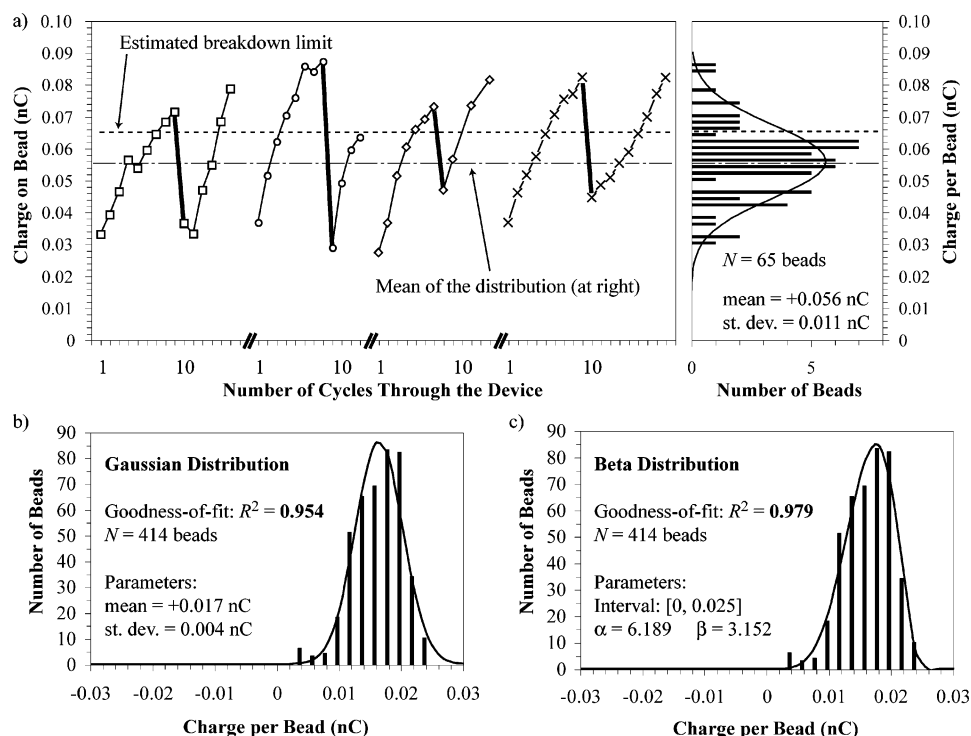


**Figure 8.** (a) The left graph shows repeated measurements of charge on four different  $450\text{-}\mu\text{m}$ -diameter microspheres with tetraalkylammonium functionality (1); the right graph shows a histogram of single measurements of charge for 65 such beads. (b) Histogram of the measurements of charge of  $200\text{-}\mu\text{m}$ -diameter microspheres with tetraalkylammonium functionality (1), fit with a Gaussian distribution. (c) The same histogram shown in panel b, fit with a  $\beta$ -distribution.

Humidity plays a complicated role in the discharge of electrets. The threshold for dielectric breakdown of air increases slightly with humidity: the dielectric strength of air at room temperature increases by about 2% when the relative humidity is increased from 40% to 95%.<sup>44</sup> This observation suggests that slightly greater charge could be stored under humid conditions than under dry conditions before the onset of breakdown. Surface conductivity, on the other hand, increases substantially with humidity, as conductive layers of water form on solid surfaces.<sup>25</sup> We compared the charges on electret microspheres charged at three different levels of humidity: in dry nitrogen, at 40% RH, and at 80% RH (Figure 7b). The limiting charge at 40% RH was comparable to that observed in dry nitrogen, but the limiting charge at 80% RH was about 35% less than that observed in dry nitrogen. Note that the charge observed under ambient conditions on different days (Figure 5a) also varied by  $\sim 35\%$ . We speculate that at high humidity, the layer of adsorbed water on the surface of these microspheres makes the surface more conductive than at low humidity (presumably through ionic conductivity). Under these conditions, charge on a sphere can dissipate when that sphere comes in contact with another surface. Other reports have found an increase in the rate of contact electrification with increased humidity,<sup>55</sup> or a maximum in contact electrification for moderate humidity, with less contact electrification under very dry or very moist conditions.<sup>50</sup>

**The Phenomenon of Dielectric Breakdown Explains the Broad Distribution of Charge.** To understand better the electrical discharge of these microspheres, we built a modified version of our charge-measuring device that could measure repeatedly the charge on a single bead as it traveled through a

long tube. The new device had a 16-meter-long polyethylene tube that looped 25 times through two charge-measuring concentric cylinders. (Figure S6 in the Supporting Information has a schematic and photograph of this device.) Because the flow of air through this tube resulted from the drop in pressure between atmospheric pressure and house vacuum over a distance of 16 meters, the average velocity of air was slower in this device ( $\sim 8$  m/s) than in the other device ( $\sim 70$  m/s). The Reynolds number was  $\sim 450$ , within the regime of laminar air-flow. The flow of air drew a single charged bead through the tube, and the charge-measuring cylinders (connected to an electrometer) measured the charge on that bead 25 times as it traversed the coiled 16-meter tube. Presumably, the laminar flow of air reduced the frequency of collisions between the bead and the walls of the tube, although some collisions still occurred because the path of the bead through the coiled tube was not straight. In addition, the slower flow of air (compared with the other device) meant that a bead would sometimes adhere to the side of the tube and stop moving; applying a “puff” of pressurized nitrogen dislodged the bead and allowed it to move again. Typically, a bead passed through the charge-measuring cylinders every 0.5 s.

With this device, we can study the kinetics of contact electrification of an uncharged bead; we will report on such kinetic measurements in a subsequent publication. Of interest for this paper is our direct observation of electrical discharges (Figure 8a). The graph on the left shows examples of repeated measurements of the charge of a single positively charged,  $450\text{-}\mu\text{m}$ -diameter microsphere as it cycled through the device. (The four separate curves on that graph represent four different beads.) The charge on each bead gradually increased with each cycle through the device, sharply decreased in a single cycle

(55) Wiles, J. A.; Fialkowski, M.; Radowski, M. R.; Whitesides, G. M.; Grzybowski, B. A. *J. Phys. Chem. B* **2004**, *108*, 20296–20302.

(highlighted in bold on the graph), and gradually increased again. These results show the charging of the bead by contact electrification between the bead and the polyethylene tube, interrupted by a discharge event that presumably results from the breakdown of air. (We note that the rate of charging of beads in this device is much slower than that observed in the other device, presumably because the turbulent flow of air in the other device results in more frequent contacts between the bead and the polyethylene tube.) The dotted line on the graph shows the threshold for dielectric breakdown (estimated by eq 1). In each case the charge on a bead increases to some amount above that limit, and then the discharge reduces the charge to significantly below that limit. The initiation of a breakdown event requires the adventitious presence of a gaseous ion or electron in the region of high electric field near a bead,<sup>44</sup> and the cascading ionization of the gas is a highly nonlinear process, so each breakdown event is different.

The somewhat random nature of these breakdown events can explain the broad distributions we observe for these charged electret microspheres. The histogram at the right in Figure 8a shows the distribution of charges for 65 of the same 450- $\mu\text{m}$ -diameter positively charged beads, measured using our usual device. Note that the range of charges observed during repeated measurements of single beads (the graph on the left) is comparable to the range of charges observed for single measurements on many beads (the graph on the right).

To determine better the shape of this distribution, we measured the charge on 414 individual 200- $\mu\text{m}$ -diameter positively charged microspheres using our usual charge-measuring device. Figure 8b shows the histogram of these measurements, along with the best-fit Gaussian curve. The Gaussian distribution cannot model the slight but obvious skewness in the experimental data. Figure 8c shows the same experimental data fit with a beta distribution.<sup>56</sup> The parameters of the beta distribution have no physical significance, but this distribution fits the skewed experimental data better than the Gaussian distribution does. Indeed, most of our measurements of charge show skewed distributions, although the distributions are not all skewed in the same direction. Considering the observations of dielectric breakdown in Figure 8a, we believe these skewed distributions are physically meaningful: the two tails of the distribution result from different physical phenomena, so we should not expect the distribution to be symmetric. In this case, above the breakdown limit, the distribution tails off relatively quickly, as beads with charges above this limit are inherently unstable and will eventually suffer a breakdown event. Below the breakdown limit, there is a relatively long tail, as each breakdown event reduces the charge on a bead to far below the limit; one of the examples in Figure 7a shows a discharge to less than half of the breakdown limit.

**Fabrication of Ionic Electrets from Glass Microspheres.** We functionalized the surface of 250- $\mu\text{m}$ -diameter glass microspheres with silanes<sup>57</sup> to determine if the ion-transfer mechanism could be applied to materials other than polymers and to examine a system in which the ionic functional groups were confined to the surface, rather than being distributed throughout the bulk of the material. An alkyltrimethylammonium

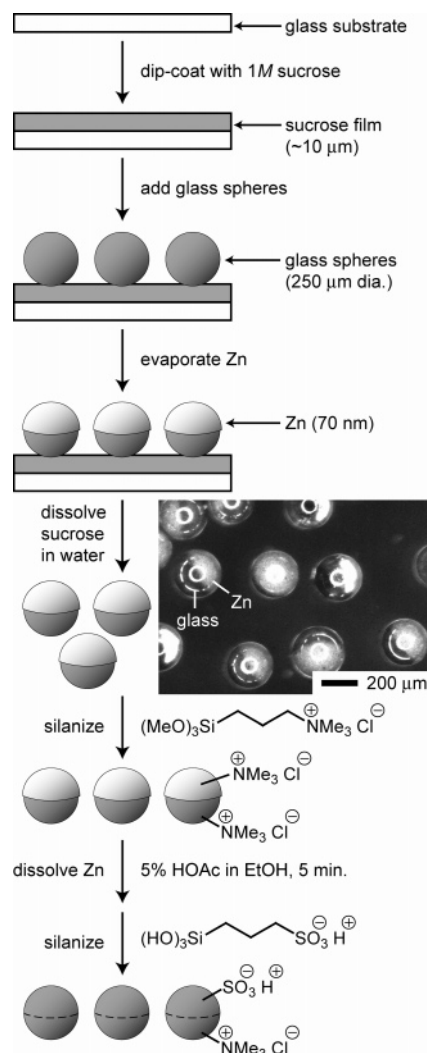


**Figure 9.** Schematic representation of the procedure for fabricating glass beads with half-and-half functionality: half of the bead has covalently bound sulfonate groups, while the other half has covalently bound alkyltrimethylammonium groups. The inset shows a dark-field optical micrograph of glass beads that are half-coated with zinc. The micrograph shows that the edges of the zinc are rough, unlike the sharp edges shown in the schematic.

chloride-containing silane generated a surface with covalently bound cations, and an alkylsulfonic acid-containing silane yielded a surface with covalently bound anions (the Experimental Section provides details). We also hypothesized that we could prepare glass spheres that would have *zero* overall charge (but a net electric dipole) if one hemisphere had bound cations and the other hemisphere had bound anions. Figure 9 shows the process used to fabricate these “half-and-half” glass microspheres: we thermally evaporated a sacrificial layer of zinc to coat half of each sphere, silanized the other half of the glass sphere with an alkyltrimethylammonium chloride silane, dissolved the zinc with 5% acetic acid in ethanol, and silanized the newly exposed glass surface with an alkylsulfonic acid silane.

Figure 10 shows histograms of the measurements of charge of these three types of silane-functionalized glass microspheres. As predicted by the ion-transfer mechanism, the spheres with bound cations all charged positively, while the spheres with bound anions all charged negatively. The surface charge density

(56) Evans, M.; Hastings, N.; Peacock, B. *Statistical Distributions*, 3rd ed.; John Wiley and Sons: New York, 2000.

(57) Oncllin, S.; Ravoo, B. J.; Reinhoudt, D. N. *Angew. Chem., Int. Ed.* **2005**, *44*, 6282–6304.

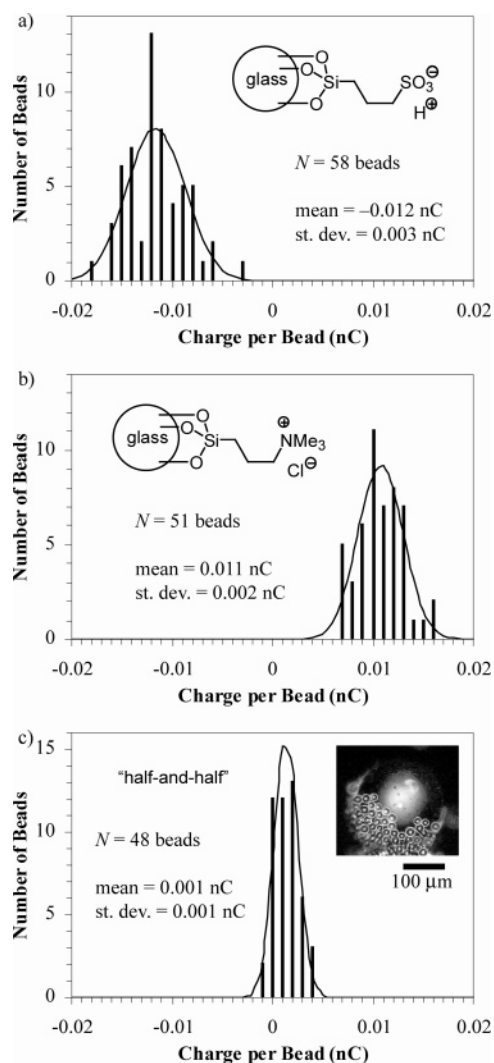


**Figure 10.** Histograms (charge per bead) for glass beads (250- $\mu\text{m}$  diameter) charged by contact with aluminum. The half-and-half beads (c) had half of their surface functionalized with sulfonate as in panel a and half functionalized with tetraalkylammonium as in panel b. The inset in panel c shows the selective adhesion of positively charged 20- $\mu\text{m}$ -diameter microspheres to only one hemisphere of the half-and-half glass beads.

(about one elementary charge per 2000  $\text{nm}^2$ ) was similar to that of the polystyrene-based ionic electrets.

The “half-and-half” spheres had approximately zero overall charge, as predicted. The small charge of these beads confirms our earlier observation that the surface charge density of positively charged ionic electrets is similar to that of negatively charged ionic electrets. We note that the standard deviation of the charge on the “half-and-half” spheres is about three times smaller than the standard deviations of other types of spheres; this observation suggests that the broad distribution of charge of the other ionic electrets is not merely an artifact of our charge-measuring device. We used electrostatic self-assembly<sup>18</sup> to image the distribution of charge on these spheres. The glass beads were agitated with 20- $\mu\text{m}$ -diameter tetraalkylammonium-functionalized polystyrene microspheres (**1**) in a glass dish. The small microspheres became positively charged by contact electrification and adhered only to the negatively charged regions of the glass beads. As shown in the inset in Figure 10c, the microspheres adhered to roughly half of the glass bead; this

observation confirms that each glass bead was roughly half negatively charged and half positively charged.

**Patterning of Charge on a Planar Ionic Electret.** We hypothesized that patterns of chemical functionality on a surface, with bound cations in one region and bound anions in another, would yield patterns of charge on that surface. Silanes can be patterned on oxide surfaces using photolithography,<sup>58–60</sup> focused ion beams,<sup>61</sup> scanning-probe techniques such as dip-pen nanolithography,<sup>62,63</sup> and soft lithography.<sup>45,64,65</sup> We used microcontact printing,<sup>66</sup> a type of soft lithography, to pattern silanes on a silicon wafer with a 300-nm layer of thermally grown oxide. Figure 11a shows our approach: we spin-coated a solution of alkyltrimethylammonium silane on a gold “inker pad”, which we used to “ink” a topographically patterned PDMS stamp. We stamped this silane on the  $\text{SiO}_2$  surface, cured the silane layer, treated the rest of the surface with an alkylsulfonic acid silane, and imaged the resulting patterns of charge by KFM.<sup>46–48</sup> (Since the sulfonic acid was deposited from a water/ethanol mixture, the sulfonic acid is probably dissociated into sulfonate and  $\text{H}_3\text{O}^+$ .) The KFM image (Figure 11b) shows the pattern of surface potential; the topography (Figure 11c) was essentially flat. The regions with covalently bound cations had a more positive potential, while the regions with covalently bound anions had a more negative potential. These patterns were stable for several days under ambient conditions; we did not investigate their long-term stability. We cannot calculate the charge density on the surface from these measurements of surface potential, because the KFM technique measures the relative surface potential between different locations on the surface, rather than the absolute electric field above the surface. We presume that the net charge in this case also results from the loss of some mobile counterions during the preparation and washing of the sample; this may be an example of contact electrification between the solid and the washing liquid (ethanol).<sup>6</sup>

**Patterning of Charge on Glass Microspheres.** The use of soft materials such as PDMS enables patterning of nonplanar surfaces;<sup>45</sup> we used this feature of soft lithography to pattern regions of charge on 250- $\mu\text{m}$ -diameter glass microspheres. Figure 12a shows the procedure: we clamped a single layer of glass microspheres between a slab of PDMS and a glass slide and immersed the entire assembly in a solution of alkyltrimethylammonium-containing silane. The PDMS conformally contacted a small region around the “north pole” of each sphere, and prevented the silane from reacting with that region. After removing the beads, we silanized the newly exposed north pole region with an alkylsulfonic acid-containing silane. The resulting patterns of charge cannot be imaged using KFM, which requires flat, conductive substrates. Instead, we used electrostatic self-assembly<sup>18</sup> to image the region of charge around the north pole.

- (58) Dulcey, C. S.; Georger, J. H.; Krauthamer, V.; Stenger, D. A.; Fare, T. L.; Calvert, J. M. *Science* **1991**, 252, 551–554.
- (59) Sugimura, H.; Ushiyama, K.; Hozumi, A.; Takai, O. *Langmuir* **2000**, 16, 885–888.
- (60) Calvert, J. M. *J. Vac. Sci. Technol., B* **1993**, 11, 2155–2163.
- (61) Ada, E. T.; Hanley, L.; Etchin, S.; Melngailis, J.; Dressick, W. J.; Chen, M. S.; Calvert, J. M. *J. Vac. Sci. Technol., B* **1995**, 13, 2189–2196.
- (62) Ivanisevic, A.; Mirkin, C. A. *J. Am. Chem. Soc.* **2001**, 123, 7887–7889.
- (63) Pena, D. J.; Raphael, M. P.; Byers, J. M. *Langmuir* **2003**, 19, 9028–9032.
- (64) Jeon, N. L.; Finnie, K.; Branshaw, K.; Nuzzo, R. G. *Langmuir* **1997**, 13, 3382–3391.
- (65) Geissler, M.; Kind, H.; Schmidt-Winkel, P.; Michel, B.; Delamarche, E. *Langmuir* **2003**, 19, 6283–6296.
- (66) Kumar, A.; Biebuyck, H. A.; Whitesides, G. M. *Langmuir* **1994**, 10, 1498–1511.



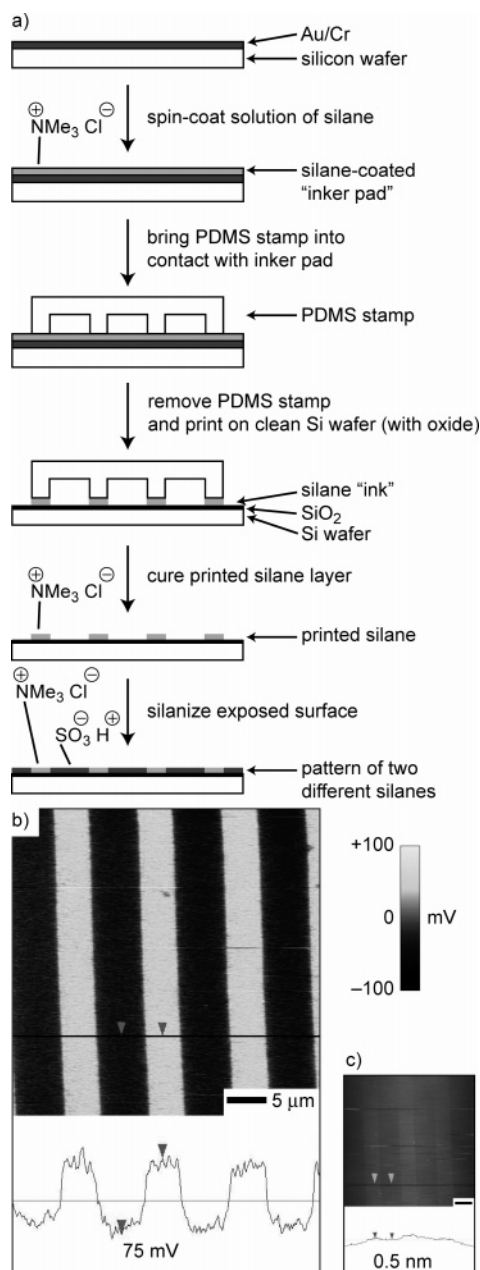


**Figure 11.** (a) Schematic representation of the procedure for microcontact printing of silanes on a silicon surface using a patterned PDMS stamp and a gold "inker pad." (b) KFM image of the surface electrostatic potential for a silicon surface that has been patterned with silanes. The surface potential is negative in the regions with the alkylsulfonate (–) silane and positive in the regions with the tetraalkylammonium (+) silane. (c) AFM image of the topography of the same region shown in part b. The regions of positive surface potential are very slightly raised (<1 nm) above the background. (Deposition of silanes often leads to multilayers; an AFM image of the printed silane layer taken before deposition of the second silane showed that the printed layer is ~2 nm thick.)

The glass beads were agitated with 20- $\mu$ m-diameter tetraalkylammonium-functionalized polystyrene microspheres (**1**) in an aluminum dish. The small microspheres became positively charged by contact electrification and adhered only to the negatively charged regions of the glass beads. As shown in Figure 12 parts b, c, and d, the microspheres adhered only to the small north pole region on each bead; this observation confirms that each glass bead had a small region of negative charge.

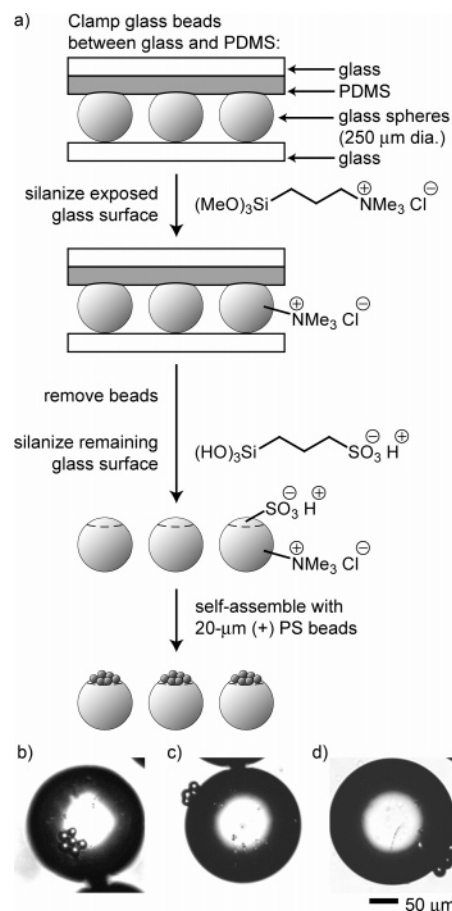


**Figure 12.** (a) Schematic representation of the procedure for patterning silanes on the surface of glass beads. The PDMS blocks the tetraalkylammonium silane from reacting with a region around the north pole of each bead. (b–d) Optical micrographs (all on the same scale) of three different self-assembled structures. The selective adhesion of the small positively charged beads to a small region on each large bead shows that the negative charge on the surface of each large bead is confined to that region.

## Conclusion

We fabricated ionic electrets from monodisperse microspheres made of crosslinked polystyrene or glass and measured the charges on individual microspheres to show that charge was proportional to surface area. The ion-transfer model correctly predicted the sign of charge that these electrets acquired through contact electrification, and the dielectric breakdown of air limits the magnitude of charge. We extended this technique to pattern regions of charge on the surface of silicon (with oxide) and on glass microspheres.

These results demonstrate that the ion-transfer mechanism offers a rational approach to materials that bear a net electrostatic charge. The dielectric breakdown of air imposes a universal limit on the stable charge on an electret, and the charges on these ionic electrets are close to this limit; thus, other methods of charging, such as bombardment with an electron-beam, cannot create stable spherical electrets with more charge than these ionic electrets. These materials could replace electrets that are currently charged using an electron-beam or ion-beam, such as the space-charge electrets used in microphones. In addition, our preparation of half-and-half glass microspheres that acquired no net electrical charge suggests a possible strategy for making new materials that do not develop a net charge upon contact but may develop dipoles or higher multipoles instead.



In principle, any insulating material that has covalently bound ions and mobile counterions at its surface can function as an ionic electret. The presence of adsorbed water facilitates the dissipation of charge: for maximum charge, the humidity should be low, and hydrophilic materials, such as ion-exchange resins, should not be used. There are two possible methods that one could use to overcome the limit imposed by the dielectric breakdown of air: the use of gases with a greater dielectric strength, such as SF<sub>6</sub>, or the use of high vacuum (the threshold for field emission in vacuum is about 10 times greater than the threshold for dielectric breakdown of air).<sup>6</sup>

Although there is considerable experimental support for the ion-transfer model of contact electrification, the atomic-level mechanistic details remain obscure. There have been no detailed theoretical studies of this ion-transfer mechanism. No one has applied the classical tools of mechanistic organic chemistry (temperature effects, isotope effects, etc.), nor used any of the powerful experimental methods for probing reactions on surfaces, in the study of contact electrification of ionic electrets. Because we focused this paper on understanding and achieving the *maximum* charge on these materials, we found that the chemistry of the material had no impact on the charging: only the dielectric breakdown strength of the surrounding medium had an effect. Studies of the kinetics of contact electrification *below* the breakdown limit should offer more information about the fundamental ion-transfer mechanism of contact electrification. For instance, we would like to know the relative contributions of entropy and enthalpy to the transfer of ions from one surface to another. Moreover, the fundamental mechanism of contact electrification of nonionic materials (e.g., contact between PTFE and Nylon) remains unknown, after more than a century of research. We hope that a recent renewal of interest in this subject,<sup>1–3,37,55</sup> particularly within the chemistry community, will offer some new insight into this ancient question.

## Experimental Section

**General.** Unless otherwise specified, all chemicals and solvents were purchased from Aldrich and used as received. Elemental analyses were performed by Galbraith Laboratories, Inc. (Knoxville, TN). The preparation of chloromethylated crosslinked polystyrene microspheres and their tetraalkylammonium (**1**) and azo-sulfonate (**4**) derivatives was described in our recent communication.<sup>18</sup>

**Preparation of Sulfonate Beads, 2.** Chloromethylated polystyrene was sulfonated using a literature procedure.<sup>67</sup> Briefly, the beads were allowed to react with dimethylsulfide in methanol to yield the resin-bound sulfonium salt. This resin was sufficiently polar that it could be swelled with aqueous sodium sulfite; the sulfite substituted for the dimethylsulfonium moiety, yielding the resin-bound sulfonate. IR (KBr):  $\nu_{\text{S=O}}$  1179 and 1037 cm<sup>-1</sup>. Anal. Found: C, 79.09; H, 7.41; S, 3.34.

**Preparation of Alkyltriphenylphosphonium Beads, 3.** To 10 mL of *N*-methylpyrrolidinone (NMP) was added 100 mg of chloromethylated polystyrene beads and 200 mg of triphenylphosphine. The mixture was stirred at 100 °C for 5 days. The beads were collected by filtration, washed twice with 20-mL portions of ethanol, twice with 20-mL portions of DMF, three times with 20-mL portions of THF, and three times with 20-mL portions of ethanol. The resulting colorless beads were dried in an oven at 60 °C and stored in a glass vial under ambient conditions. IR (KBr):  $\nu_{\text{P-P}}$  1018 and 1110 cm<sup>-1</sup>. Anal. Found: C, 82.84; H, 7.01; P, 0.48. The low P content suggests that the reaction

was only ~20% complete. The reaction of triphenylphosphine with chloromethylated polystyrene is known to be quite slow,<sup>68</sup> and the crosslinked polystyrene purchased from Duke Scientific is ~10% crosslinked, whereas typical solid-phase synthesis resins are ~1% crosslinked. The highly crosslinked beads swell in NMP to only ~1.5 times their volume, while the usual beads swell to about 10 times their volume. The high degree of crosslinking may have prevented the bulky triphenylphosphine nucleophile from reacting throughout the bead.

**Charge-Measuring Apparatus.** The charge on each bead was measured using the apparatus depicted in Figure 2a. A polyethylene tube (2 mm diameter) was connected to house vacuum and threaded through three concentric aluminum cylinders. The three concentric cylinders were approximately 4, 9, and 30 mm in diameter and 1.0, 1.1, and 1.4 meters in length, respectively. Concentric solid polyethylene tubing insulated the cylinders from each other. The three cylinders were soldered to the three leads of a triaxial shielded cable (Belden 9222), with the innermost cylinder connected to the central lead; these connections were all enclosed within the outermost shielding cylinder. This shielding configuration was necessary in order to make measurements with low noise (rms noise ~20 fC) and minimal background drift. The triaxial cable was connected directly to a Keithley model 6514 electrometer in charge-measurement mode: in this mode, the instrument acts as a current integrator. The total charge (time integral of the current) was recorded 60 times per second on a computer connected to the electrometer. The main text describes the analysis of these data. (Figure S5 in the Supporting Information provides a schematic illustration and photograph of this device.)

**Apparatus for Repeated Measurements of Charge on a Single Bead.** A polyethylene tube (PE-100, 16 meters long, 0.86 mm i.d., 1.52 mm o.d.) was looped 25 times (radius of loops: 10 cm) through two concentric curved metal cylinders: the inner cylinder was a flexible steel spring (22 cm long, 1.4 cm i.d., 1.8 cm o.d.) and the outer cylinder was fashioned from curved iron pipe (30 cm long, 2.5 cm i.d., 3.4 cm o.d.). One end of the polyethylene tube was connected to house vacuum. The two metal cylinders were electrically insulated from one another by concentric PVC tubing. The cylinders were connected to a shielded triaxial cable in the same fashion as the other charge-measuring device. The entire apparatus was electrically shielded with aluminum foil. Data was collected and analyzed as with the other device. (Figure S6 in the Supporting Information provides a schematic illustration and photograph of this device.)

**Silanization of Glass Beads.** Glass microspheres (250- $\mu$ m diameter, Supelco) were immersed in a 10% solution of the desired silane (Gelest) in 95% ethanol. The solution was adjusted to pH ~5 with acetic acid. After 10 min, the beads were rinsed once with ethanol and heated at 60 °C for at least 1 h. The beads were then rinsed three times with ethanol and dried at 60 °C. The silanes were *N*-trimethoxysilylpropyl-*N,N,N*-trimethylammonium chloride and 3-(triethoxysilyl)-1-propanesulfonic acid.

**Fabrication of Half-and-Half Glass Beads.** A glass microscope slide was dip-coated with a 1 M aqueous solution of sucrose and dried at 60 °C for 20 min. The dry sucrose film was made tacky by moistening it slightly with water vapor from exhaled breath. Glass microspheres (250- $\mu$ m diameter, Supelco) were poured onto the surface; a single layer of beads adhered to the tacky sucrose film (the beads did not appear to sink into the film). A thin film of zinc (~70 nm) was evaporated thermally onto the glass microspheres. The half-zinc-coated beads were released by dissolving the sucrose in water.

The beads were washed with ethanol, silanized with *N*-trimethoxysilylpropyl-*N,N,N*-trimethylammonium chloride (10% in ethanol, no acid added), and heated at 60 °C for at least 1 h. The beads were treated for 10 min with an ethanolic solution containing 10% 3-(triethoxysilyl)-1-propanesulfonic acid and 5% acetic acid. This solution was sufficiently acidic to dissolve the zinc (~5 min); it also served to silanize

(67) Doescher, F.; Klein, J.; Pohl, F.; Widdecke, H. *Makromol. Chem.* **1982**, *183*, 93–102.

(68) Frechet, J. M.; Schuerch, C. *J. Am. Chem. Soc.* **1971**, *93*, 492–496.

the newly exposed glass surface. The beads were washed once with ethanol and dried at 60 °C. To image the distribution of charge on these glass beads, we combined in a glass dish ca. 0.5 mg of 20- $\mu$ m-diameter polystyrene microspheres with tetraalkylammonium functionality (**1**) with ca. 30 of the glass microspheres with half-and-half surface charge. The dish was agitated manually for 30 s. Each glass bead had a disordered, incomplete monolayer of 20- $\mu$ m polystyrene spheres adhered to roughly one-half of the bead, as shown in the inset in Figure 10c.

**Patterning of Silanes on a Silicon Surface.** Silanes were printed on a silicon surface (with oxide) using microcontact printing.<sup>45</sup> Poly-(dimethylsiloxane), PDMS (Dow Corning, Sylgard 184), was poured over a photolithographically fabricated master. After curing at 65 °C for 2 h, the PDMS was oxidized in an oxygen plasma for ~60 s and silanized with the desired silane (1% *N*-trimethoxysilylpropyl-*N,N,N*-trimethylammonium chloride in 95% ethanol/water). The stamp was washed thoroughly with ethanol and dried with a stream of N<sub>2</sub>. A 0.05% solution of the same silane in ethanol was spin-coated on a gold “inker pad”<sup>65</sup> (a silicon wafer with ~5 nm of Cr and ~70 nm of Au) at 3000 rpm for 30 s. The silanized PDMS stamp was “inked” by contact with this inker pad for 60 s. The stamp was then placed for 30 s on a plasma-cleaned silicon wafer with a ~300 nm thermally grown oxide layer (Universitywafer.com). This silanized wafer was allowed to sit at room temperature for 2 h and then immersed in a 1% solution of 3-(trihydroxysilyl)-1-propanesulfonic acid in 95% ethanol/water for 10 min. The wafer was washed thoroughly with ethanol and dried with a stream of N<sub>2</sub>.

**Surface Potential Measurements.** The surface topography and surface potential were imaged with an AFM (D3100, NSIV; Digital Instruments). The topographic images were obtained using the AFM in tapping mode and the KFM images were obtained using the AFM in surface potential mode.

**Patterning of Silanes on Glass Microspheres.** A glass microscope slide was coated with a ~1 mm layer of PDMS (Sylgard 184, Dow

Corning). Glass microspheres (250- $\mu$ m diameter, Supelco) were clamped between this PDMS-coated slide and a plain glass microscope slide. The PDMS conformed to a small spot around the north pole of each sphere. The spheres were immersed in a solution of *N*-trimethoxysilylpropyl-*N,N,N*-trimethylammonium chloride (10% in ethanol, adjusted to pH~5 with acetic acid) for 10 min. The spheres were washed once with ethanol and the silane layer cured at 60 °C for 1 h. The beads were removed, washed again with ethanol, and silanized with a solution of 3-(trihydroxysilyl)-1-propanesulfonic acid (10% in ethanol, adjusted to pH ~5 with acetic acid). The beads were washed three times with ethanol and dried at 60 °C.

**Self-Assembly on Glass Microspheres with Patterned Charge.** Following the procedure reported in our recent communication,<sup>18</sup> we combined in an aluminum dish ca. 0.5 mg of 20- $\mu$ m-diameter polystyrene microspheres with tetraalkylammonium functionality (**1**) with ca. 30 of the glass microspheres with patterned surface charge. The dish was agitated manually for 30 s. Most of the glass spheres had a small “clump” of adherent 20- $\mu$ m beads (as shown in Figure 11b); about a quarter of the glass spheres had no adherent beads.

**Acknowledgment.** This research was supported by the Army Research Office (Grant W911NF-04-1-0170) and used the shared Resource Facilities supported by the National Science Foundation under NSEC (PHY-0117795) and MRSEC (DMR-0213805) awards. The authors would like to thank Dr. Emily Weiss for assistance with the KFM measurements.

**Supporting Information Available:** Histograms of the measurements of charge for all experiments discussed in the article, and photographs of the two devices used to measure charge on single microspheres. This material is available free of charge via the Internet at <http://pubs.acs.org>.

JA067301E